Kinetics and design of distillation reactor with ZSM-5@SiC foam catalytic packing for ethyl levulinate synthesis in industrial scale

Qiuyan Ding[1] | Hong Li[1] | Zihao Chen[1] | Yanan Guan[2] | Xingang Li[1] | Jinsong Zhang[2] | Yilai Jiao[2,*] | Jing Zou[3] | Xin Gao[1,*]

[1]School of Chemical Engineering and Technology, National Engineering Research Center of Distillation Technology, Collaborative Innovation Center of Chemical Science and Engineering (Tianjin), Tianjin University, Tianjin 300072, China

[2]Institute of Metal Research, Chinese Academy of Sciences, 72 Wenhua Road, Shenyang 110016, China

[3]The State Key Laboratory of Precision Measuring Technology and Instruments, Tianjin University, Tianjin 300072, China

Corresponding authors: gaoxin@tju.edu.cn (X. Gao), yljiao@imr.ac.cn (Y. Jiao)

Abstract: Distillation reactor is one of the important equipment to improve the reaction conversion limited by the chemical equilibrium, however, the design of distillation reactor in industrial scale is still challenging due to the lack of efficient catalytic packing with corresponding kinetics. This work developed the novel catalytic packing consists of the structured ZSM-5@SiC foam catalyst and corrugated sheet, which used in distillation reactor for synthesis of ethyl levulinate (EL). The kinetic of structured ZSM-5@SiC foam catalyst was measured and model regarding the "structure factor" of ZSM-5@SiC catalyst and fluid flow conditions. Furthermore, the design of distillation reactor in industrial scale has been performed based on the developed kinetics, which demonstrated an excellent performance in the designed distillation reactor (EL yield 37.65% with energy consumption 3695 kJ/kg) are achieved. X-ray CT characterization revealed that the ZSM-5 coating thickness has the significantly effects on the kinetics and performances of distillation reactor.

KEYWORDS: ZSM-5@SiC, structured catalyst, kinetics, reactive distillation, ethyl

levulinate

1 | INTRODUCTION

As a crucial green platform chemical in levulinic acid ester manufacturing, ethyl levulinate (EL) has attracted more attention in academic and industry fields, which is widely used in solvents and essential additives.[1-4] When EL is used as a diesel additive, it can improve the lubricity and flash point of oil products[1,5] and reduce the sulfur emission from diesel engines[6]. More notably, EL is an entirely renewable bio-based product meeting low carbon and environmental protection requirements, which will achieve a massive shift away from fossil fuels to clean, renewable energy sources. Therefore, it is not surprising that the demand for EL is increasing rapidly due to great exploitable value and application prospects.

Currently, there are three main preparation methods of EL, including direct alcoholysis of biomass[7,8], levulinic acid (LA) esterification[2,4,9-13], alcoholysis of furfuryl alcohol[14]. Among them, esterification of LA and ethanol (EtOH) is the most common route for EL synthesis in the presence of acid catalysts, which has the outstanding advantages with renewable bio-based reactants, lower carbon emissions, mild reaction conditions, and fewer byproducts. However, the forward reaction is restricted by its chemical equilibrium of the esterification reaction, resulting in lower reaction conversion and product yield.[15,16] Thus, the study of novel reactor, i.e., process intensification and process integration method, is essential for further EL product in industrial scale.

RD technology is the most typical representative of process intensification by integrating catalytic reaction and distillation separation, which can break equilibrium limitations, greatly simplify processes, low capital cost and improve the yield and selectivity of the product.[17] RD

technology has been successfully applied to many reactions, such as esterification[16,18,19], hydrolysis[20,21], production of solketal[15]. Here, catalysts and catalytic packing are the core of RD technology. Heterogeneous catalysts, i.e., Zr-containing UiO-66-type MOFs[9], zeolites[2,10] and sulfated oxides[3,10], sulfated mesoporous zirconosilicates[11], ion exchange resin[4,12,13], and heteropoly acids[1,22], were widely used in the EL synthesis. Although the development of new catalysts has improved the catalytic performance and the yield of products, there are still some challenges for the catalytic packing with the reactive and separation functions. The reason is that the heterogeneous catalyst particles are made into bale-type[23,24] and splinted-type[25,26] catalytic packing in a specific way, which was loaded into the distillation reactor to realize the function of reaction and separation. However, the catalytic packings above mentioned have lower catalyst utilization and separation efficiency. The design of distillation reactor is difficult to achieve due to the limited reaction space and gas-liquid mass transfer channel.

In recent years, the structured catalytic packing (SCP) have been widely applied in the distillation reactor for the esterification reactions to effectively solving the above problems.[27,28] In particular, more and more researchers have focused on the preparation of structured catalyst over the SiC foam materials supports (SiC-FMS).[29-34] It benefits from corrosion resistance, high mechanical strength, low-pressure drop, and much higher heat and mass transfer rates,[35,36] and currently has become a popular catalytic carrier for reactive process intensification. Whereas, the reaction kinetics based on real structure is essential for industrial application, because the structure of supports and coating characteristics have a great impact, which is the basis of the design of distillation reactor. Chen et al.[37] investigated

catalytic combustion kinetics of isopropanol over ZSM-5 coating/PSSF catalyst. Methanol-to-propylene (MTP) kinetic model based on the structured SS-fiber@HZSM-5 core-shell catalyst was reported to describe monolith reactor behavior of MTP by Wen et al.[38] Kinetic studies of catalytic CO_2 methanation over the structured Ni@NaA-SiC catalysts was performed by Zhang et al.[34] There are almost no researchers to report relationship between structure of ZSM-5@SiC and kinetics for EL synthesis. Let alone, the design of distillation reactor with SCP in industrial scale is even more absent.

In this work, we developed a structured ZSM-5@SiC catalysts supported on SiC foam, which were prepared successfully using a two-step coating and steam-assisted crystallization process. The macroscopic properties of structured ZSM-5@SiC catalyst, such as macroscopic pore diameter distribution and porosity, ZSM-5 coating thickness and uniformity, were characterized by means X-ray computed tomography (CT). The effects of temperature, flow rate, average macroscopic pore diameter of structured ZSM-5@SiC catalyst (AMPD-ZSM-5@SiC), ZSM-5 coating thickness, and acid to alcohol molar ratio on the formation rate of EL were investigated. The kinetic model was established by introducing a parameter termed as ‘‘structure factor’’ based on macroscopic properties of structured ZSM-5@SiC catalyst and liquid flow rate in the reactor. Finally, the distillation reactor design with ZSM-5@SiC foam catalytic packing in industrial scale has been performed to better understand this reaction and separation process using developed kinetics model with structure factors for the LA esterification system.

2 | EXPERIMENTAL SECTION

2.1 | Synthesis of structured ZSM-5@SiC catalyst

ZSM-5 coating was prepared on the SiC-FMS using a two-step coating with steam-assisted crystallization method. SiC-FMS were boiled with 10% sodium hydroxide solution before use to expose micron-level porous layer, and then calcined at 900°C to form nano-thickness SiO_2 layer, which can be converted to form ZSM-5 zeolite in the hydrothermal synthesis reactor. The synthesis method of structured ZSM-5@SiC catalyst was developed in earlier study.[31] The first stage is that the SiC-FMS were dipped into obtained zeolite precursor sol, and that impregnation into a mixture of zeolite precursor sol and ZSM-5 crystals is for the second step. Details information about the synthesis of structured ZSM-5@SiC catalyst were described by Jiao et al.[31]

Structured ZSM-5@SiC catalysts with different structures were prepared by changing the coating times and different pore diameter of SiC-FMS. The obtained samples were marked as S-ZSM-5@SiC-4, M-ZSM-5@SiC-6, M-ZSM-5@SiC-8, M-ZSM-5@SiC-12, L-ZSM-5@SiC-13. Among them, the average pore diameter of SiC-FMS is distinguished as S, M, L, which are 0.62mm, 1.31mm, and 1.81mm respectively. The number represents coating times.

2.2 | X-ray CT studies of structured ZSM-5@SiC catalyst

X-ray CT is a non-destructive method to reconstruct the real structure of the target materials.[39] The structured ZSM-5@SiC catalyst samples (Φ20mm×50mm) were scanned using the X-ray CT scanning system jointly developed by Tianjin University and Tianjin Sanying Precision Instrument Co., Ltd.: the highest scanning voltage is 160 kV, the maximum

power is 25W, and the highest resolution is 0.5μm. Three-dimensional (3D) ZSM-5@SiC catalytic packing samples were reconstructed using the obtained two-dimensional (2D) slice grayscale images. Non-local means, the commonly used image filter algorithm, was used to preprocess gray image to reduce noise and improve image quality in our study. Furthermore, to accurately and quantitatively analyze the macroscopic real structure of ZSM-5@SiC, ZSM-5 coating thickness and uniformity, we adopted a watershed segmentation method based on the difference of gray image values[39] to segment images with high quality. The selection of segmentation threshold was constrained by experimentally measured porosity of structured ZSM-5@SiC catalyst. Finally, the software was used to quantitatively calculate the AMPD-ZSM-5@SiC, porosity and coating thickness of structured ZSM-5@SiC catalyst.

2.3 Characterizations of structured ZSM-5@SiC catalyst

The morphology and micro-structures images of structured ZSM-5@SiC catalyst were obtained from a scanning electron microscope (SEM), equipped with an energy dispersive X-ray spectrometer (EDX). Crystal phases of structured ZSM-5@SiC catalyst were recorded using the powder X-ray diffraction. The specific surface areas and porous pore properties of structured ZSM-5@SiC catalyst were measured via N_2 adsorption-desorption at 77K. The acid strength and the acid active sites of structured ZSM-5@SiC catalyst were determined using NH_3 -TPD.

2.4 Kinetics experiments

The catalytic activity of structured ZSM-5@SiC catalyst was measured for kinetic characteristics using a quartz tube reactor (diameter of 20mm) for the liquid phase esterification reaction of LA with EtOH. The schematic diagram of the experiment setup for

EL synthesis is shown in Figure 1. Details information about the experiments were described in our previous study.[40] The samples withdrawn were periodically injected through an autosampler and analyzed in a gas chromatography (PerkinElmer Clarus 690 GC). Details of GC methods are described in the supporting information.

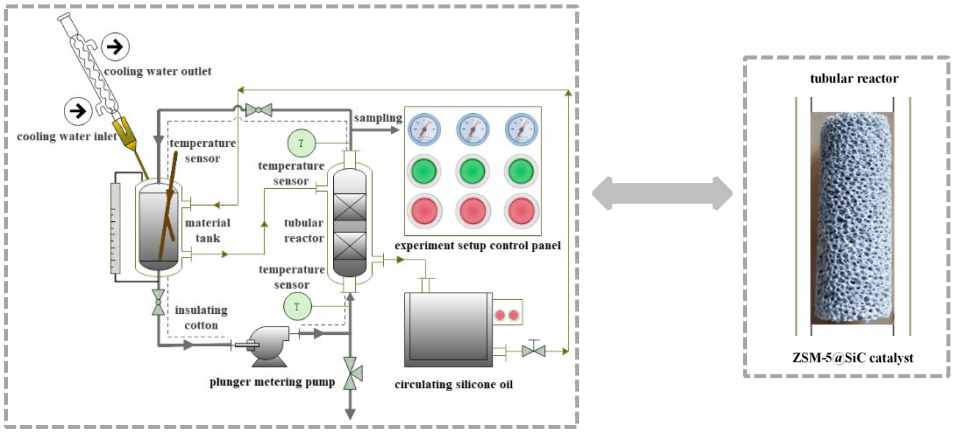

FIGURE 1 The schematic diagram of the experiment setup for EL synthesis

Observed concentrations of LA, EtOH, EL, H_2O at regular intervals were recorded under operation conditions (i.e., temperature, flow rate, AMPD-ZSM-5@SiC, ZSM-5 coating thickness, acid to alcohol molar ratio) and were input as multiresponse data. Operation conditions used for the kinetic study were listed in Table S1.

3 | STRUCTURAL CHARACTERIZATION RESULTS

3.1 | Macroscopic characterizations of structured ZSM-5@SiC catalyst

To observe and reconstruct the macroscopic real structure and the properties of structured ZSM-5@SiC catalyst, quantitative analysis of the macro pore spatial and ZSM-5 coating thickness distribution by X-ray CT is an intuitive means. 3D rendering of ZSM-5@SiC is exemplified in Figure 2(a), which indicates the uniform distribution of ZSM-5 coating on the surfaces of SiC-FMS. Moreover, divided the macroscopic pore, SiC-FMS and

ZSM-5 coating, and the segmented images are shown in Figure 2(b-d). ZSM-5 coating as the red rendering and the SiC-FMS as the green rendering, and macroscopic pore of ZSM-5@SiC as the blue rendering. Based on the above image processing, the volume fraction for each of the phases simultaneously were analyzed, as shown in Table S2. The AMPD-ZSM-5@SiC was obtained from X-ray CT images on the same threshold and segmentation, as presented in Figure S1. Based on these results, AMPD-ZSM-5@SiC of each sample were presented in Table S2.

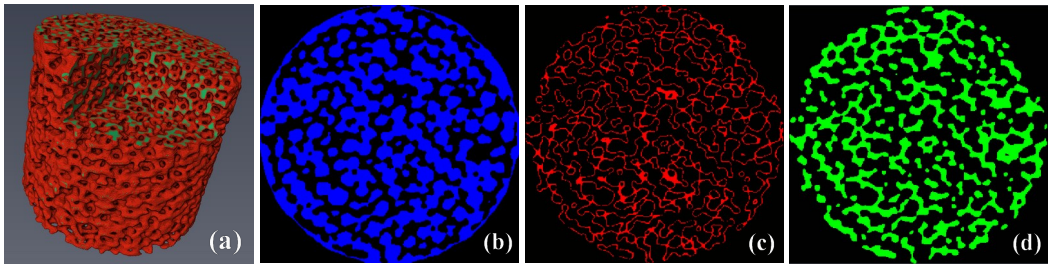

FIGURE 2 3D rendering and phase segmentation of structured ZSM-5@SiC catalyst (a) ZSM-5@SiC; (b) Macroscopic pore of ZSM-5@SiC: blue; (c) ZSM-5 coating: red; (d) SiC-FMS: green

The ZSM-5 coating thickness of structured ZSM-5@SiC catalyst is an essential parameter determining mass transfer and diffusion, affecting the possible surface reactions. Therefore, the characteristic size of the ZSM-5 coating thickness on the surfaces of SiC-FMS was measured. From the histograms in Figure S2, we can see the variation in the coating thickness for different ZSM-5@SiC samples. The average ZSM-5 coating thickness is presented in Table S2, which indicates the average thickness varies from 47.7 to 322.45μm with the increase of coating times. Nevertheless, the uniformity decreases with the increase of coating thickness from the results of the three-phase segmentation, which implies there are still some challenges to prepare structured ZSM-5@SiC catalyst with certain ZSM-5 coating

thickness and uniformity on the surfaces of SiC-FMS.

Besides, several regions of interest (ROI) in the structured ZSM-5@SiC catalyst were selected, taking M-ZSM-5@SiC-8 as an example. As shown in Figure 3, there are almost no difference between the results of ROI and the total quantitative calculation, which further confirms that the ZSM-5 coating thickness is uniform in the holistic ZSM-5@SiC sample.

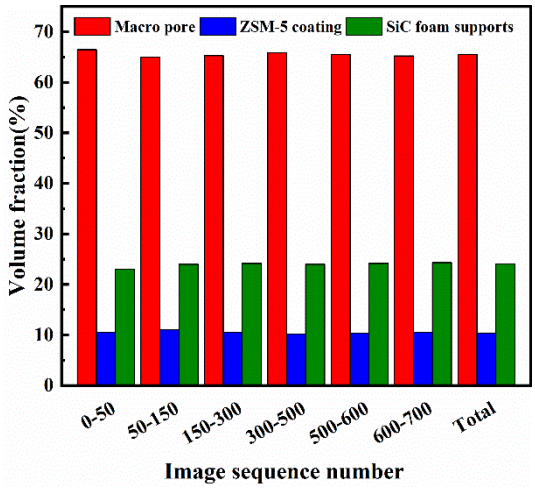

FIGURE 3 The volume fraction of the macroscopic pore, ZSM-5 coating, and SiC-FMS of ROI

3.2 | Microscopic characterizations of ZSM-5@SiC coating

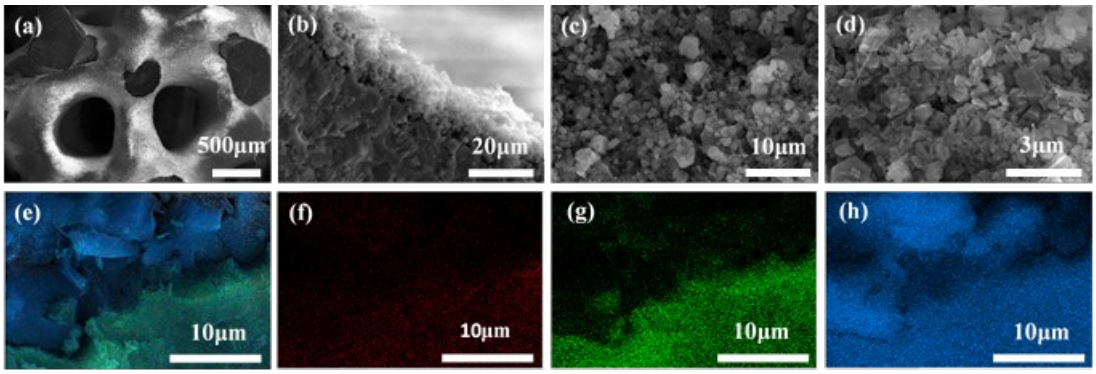

FIGURE 4 (a–d) SEM images of ZSM-5@SiC samples with different magnifications; (e–h) SEM-EDX mapping of the ZSM-5@SiC samples, Al (red), O(green), Si(blue)

The morphology of structured ZSM-5@SiC catalysts prepared with different magnifications were shown in Figure 4(a-d). It was found that, the ZSM-5 coating was

successfully grown on the surfaces of SiC-FMS, which had a thickness of around 40μm. This is consistent with the results obtained with X-ray CT. As shown in Figure 4(d), the ZSM-5 coatings prepared had twinned and intergrown crystals forming the cluster. Besides, SiC-FMS retained the original structure without the macro pores blocked, indicating the coating uniformity. EDX maps of the ZSM-5@SiC samples in Figure 4(e-h) showed that Al–O–Si (red-green-blue) phases were uniformly distributed on the SiC-FMS surface.

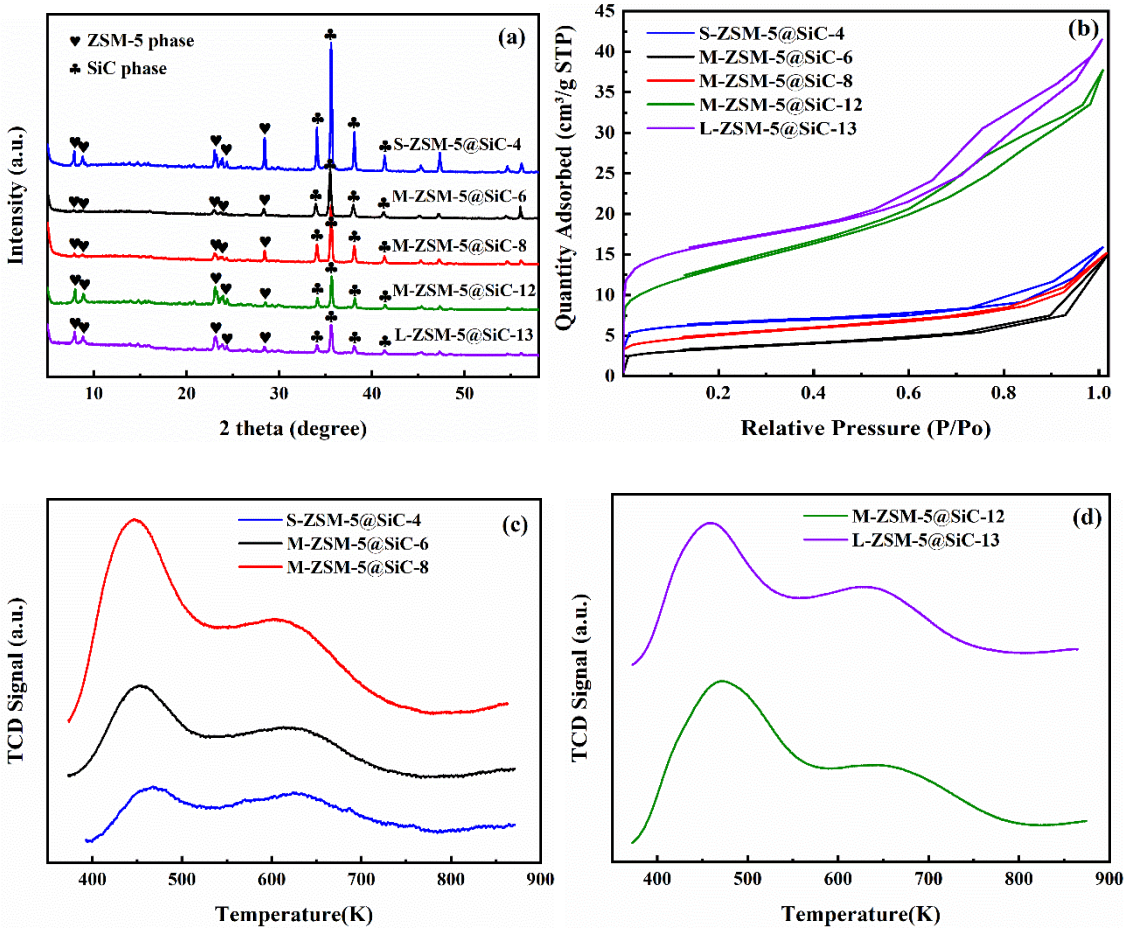

FIGURE 5 (a) X-ray powder diffraction patterns of ZSM-5@SiC samples (b) N_2 adsorption- desorption isotherms of ZSM-5@SiC samples (c-d) NH_3-TPD patterns of ZSM-5@SiC samples

XRD patterns of structured ZSM-5@SiC catalysts prepared were shown in Figure 5(a). As obvious from the XRD patterns, the typical diffraction peaks of ZSM-5 can be observed

for ZSM-5@SiC samples, proving the successful disposition of the ZSM-5 phase on SiC-FMS.[32] Compared with other structured ZSM-5@SiC catalysts, the peaks for SiC are relatively strong in the S-ZSM-5@SiC-4, indicating thinner ZSM-5 coatings on the surfaces of SiC-FMS owing to the smaller average pore diameter limitation and less of coating times.

The N_2 adsorption-desorption isotherms of structured ZSM-5@SiC catalysts were presented in Figure 5(b). The corresponding analysis data were summarized in Table S3. Here, M-ZSM-5@SiC-12 and L-ZSM-5@SiC-13 have a substantial increase in specific surface areas relative to other samples prepared. However, this presumably could be attributed to an increase in the ZSM-5 coating amount. S-ZSM-5@SiC-4 has smaller pores, which increase its specific surface areas. Moreover, All the ZSM-5@SiC samples reveal typical Type IV characteristics, which are probably related to microporous materials and mesopores materials.[30]

The acidities of structured ZSM-5@SiC catalysts were evaluated by NH_3-TPD, and Figure 5(c-d). shows the relevant patterns. It can be seen NH_3-TPD patterns exhibited two desorption peaks, representing weak acid and strong acid, respectively. Table S4 showed the desorption peak temperatures and acid active sites. Notably, the total amount of acid sites varied from 0.04 to 0.22 mmol g^{-1} due to the difference in ZSM-5 coating thickness, which will directly affect the catalytic performance of the reaction.

4 | DEVELOPMENT OF THE KINETIC MODEL

4.1 | Kinetic modeling

Pseudo-homogeneous (P-H)[18,40] and Langmuir-Hinshelwood-Hougen-Watson (LHHW)[41,42] models are commonly used in kinetic models of RD. The P-H model is simple

and has few kinetic parameters. It assumes that the temperature is the only factor that causes the difference product formation rate and the catalyst structure has no effect on the reaction rate. The main drawback of the P-H model is that it ignores the adsorption of each component on the catalyst. Therefore, the LHHW model was adopted with the surface reaction as a rate-limiting step,[42] considering the competition of the chemical species on the active sites. The activity of each component was used for the rate equation instead of concentration to accurately describe the nonideality of the liquid, which is described by Eq. (1).

$$r=\frac{k_s a_{LA} a_{EtOH}-k_s a_{EL} a_{H_2O}/K_e}{\left(1+k_{LA} a_{LA}+k_{EtOH} a_{EtOH}+k_{EL} a_{EL}+k_{H_2O} a_{H_2O}\right)^2} \quad (1)$$

The strong nonidealities mentioned above are described by means of activity coefficients γ_i, calculated with the nonrandom two-liquid (NRTL) model. Binary interaction parameters not included in the Aspen database were estimated using the UNIFAC group contribution method. The activity was calculated using Eq. (2). The activity coefficients calculation formula and related parameters are listed in Equation (S1-7) and Table S5. See supporting information for details.

$$a_i=\gamma_i c_i \quad (2)$$

where a_i is the activity of the ith components, γ_i is the activity coefficient of the ith components, c_i is the concentration of the ith components.

Ignoring adsorption effects is a crucial simplification due to the different affinities of each component to the zeolite. Schildhauer et al.[43] studied the esterification of hexanoic acid and 1-octanol on zeolite BEA. By comparing the adsorption constants of water and alcohol, it can be seen that the adsorption constant of water is about 38 times that of alcohol. Water, a

medium, is strong polar in the absence of a hydrogen-oxygen bond.[41] Due to the excellent adsorption effect of the catalyst on water, the adsorption amount of acid, alcohol, and ester can be ignored compared with water. The adsorption of water was calculated by simplifying the rate Eq. (1), as shown in Eq. (3).

$$r=\frac{k_s a_{LA} a_{EtOH}-k_s a_{EL} a_{H_2O}/K_e}{\left(1+k_{H_2O} a_{H_2O}\right)^2} \tag{3}$$

External mass transfer limitation has a significant effect on reaction kinetics due to the complex structure of ZSM-5@SiC. Thus, a parameter termed as "structure factor" was introduced into the simplified LHHW model to predict the kinetic model more accurately.

Where, k_s is the forward reaction rate constant , K_e is equilibrium constant, k_{H_2O} is the adsorption equilibrium constant of water,λ is the structure factor. The formation rate of EL can be ultimately described as:

$$r=\frac{k_s a_{LA} a_{EtOH}-k_s a_{EL} a_{H_2O}/K_e}{\left(\lambda+k_{H_2O} a_{H_2O}\right)^2} \tag{4}$$

The temperature dependence of the forward reaction rate constants and adsorption equilibrium constants in Eq. (4) were evaluated using the Arrhenius law expressed in Eqs. (S8) and (S9).

4.2 | Estimation of parameters

The parameters (kinetic parameters, adsorption equilibrium constants, and structure factors) of structured ZSM-5@SiC catalyst materials were estimated using the fourth-order Runge−Kutta integral and a least-squares method[16,44] based on the esterification reaction rate

expression Eq. (4). The optimal objective function is to minimize the square sum of the deviation between the calculated value and the experimental value. The chemical equilibrium constants are based on the data obtained in previous work[45], as shown in Eq. (S10). Furthermore, to simplify the calculation, we carried out a two-step fitting for the estimation of parameters. In the first step, the forward reaction rate constants, adsorption equilibrium constants and structure factors were evaluated using experimental data obtained under the same fluid flow situations with different temperatures. Next, the fitting equations of the forward reaction rate constants and adsorption equilibrium constants were substituted into the expression of the esterification reaction rate to obtain the structure factors under other reaction conditions.

4.2.1 | Estimation results of the model parameters

The catalytic performances were tested under different temperatures to understand further the kinetics behaviors of structured ZSM-5@SiC catalyst. Esterification reactions were investigated at 340.13, 348.13, and 356.13 K keeping other conditions constant. From Figure 6(a), it can be clearly seen that the EL formation rate gets greatly enhanced as the reaction temperature increases. The concentration of EL has more than doubled with an increase in temperature from 340.13 to 356.13K, which indicates that the temperature has a significant effect on the reaction rate. This result is very common, which is in according with the general phenomenon of reaction kinetics and also the experimental result reported in literature.[12] Above the experimental data were fitting by means of Eq. (4) to obtain the forward reaction rate constants, adsorption equilibrium constants and structure factors.

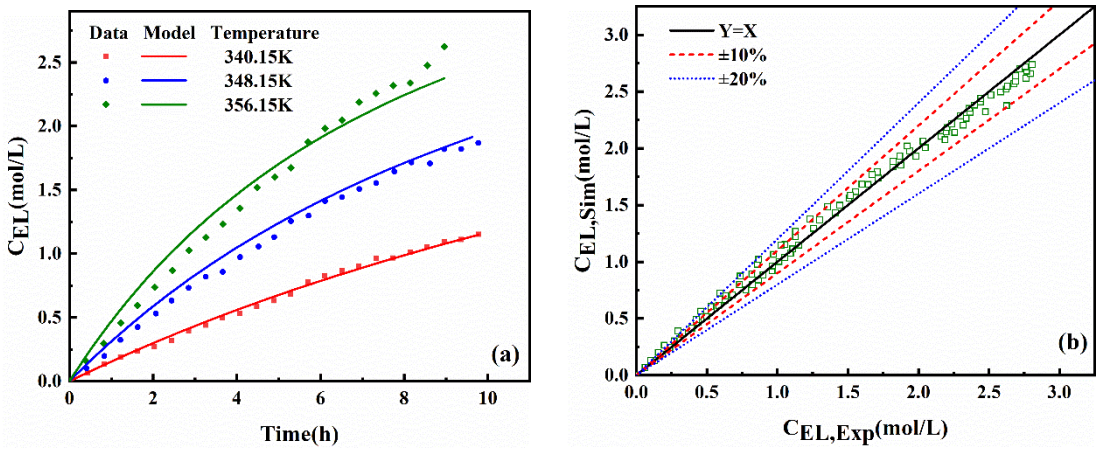

FIGURE 6 (a) Effect of the temperature on C_{EL}. (Points are experimental data, while solid lines are model prediction, Experimental conditions: Flow rate =3.5L/h, Structured catalyst: M-ZSM-5@SiC-12, LA/EtOH=1:1) (b)Plots of simulated concentration value of EL and the experimental data under different temperatures

Estimation results of parameters at different temperatures were listed in Table S6. Here, structure factors were thought to be variables related to liquid flow rate and the structure of ZSM-5@SiC catalyst. Therefore, the estimated structural factors are considered invariable as the temperature changed according to estimation results. Figure 6(b) shows the comparison between the simulated concentration value of EL and the experimental data. It can be seen that most of the data collected by the experiments are within the error window of ±10%, and a few data points are within the error window of ±20%, indicating that the experimental data are in good agreement with the model prediction.

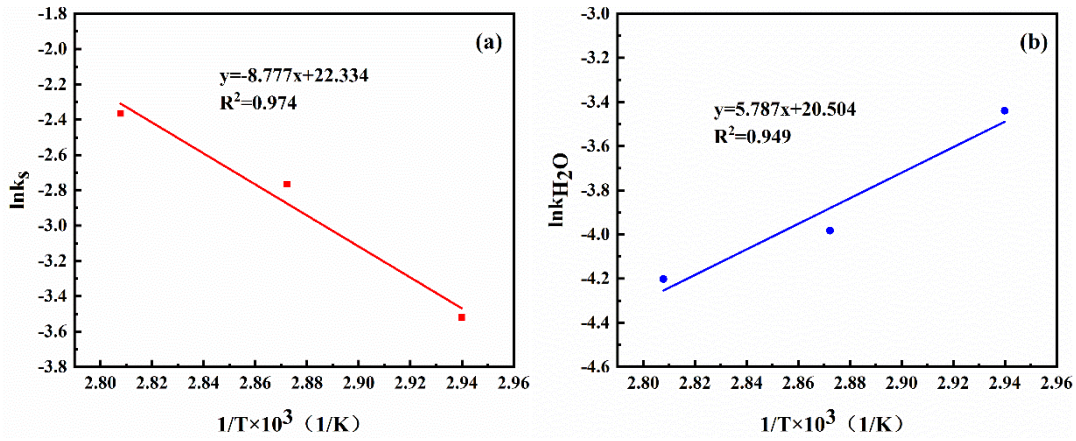

FIGURE 7 (a) The temperature dependence of the forward reaction rate constants; (b)The temperature dependence of the adsorption equilibrium constants

As shown in Figure 7(a-b), the logarithm of the forward reaction rate constants and adsorption equilibrium constants of EL is linearly related to the reciprocal of absolute temperature (1/T), and linearity is high. Consequently, the temperature dependence of the forward reaction rate constants and adsorption equilibrium constants were evaluated using Eqs. (S8) and (S9). The results are described as:

$$k_s = 5.006 \times 10^{9} \exp^{\left(\frac{-8776.6}{T}\right)} \tag{5}$$

$$k_{H_2O} = 1.245 \times 10^{-9} \exp^{\left(\frac{5787.5}{T}\right)} \tag{6}$$

Furthermore, the structure of ZSM-5@SiC catalyst is also a crucial factor affecting the reaction kinetics of EL. The catalytic performances were carried out with ZSM-5@SiC materials as the catalyst, investigating a wide range of operation conditions (i.e., flow rate, AMPD-ZSM-5@SiC, ZSM-5 coating thickness, LA to EtOH molar ratio). The EL formation rate results, as shown in Figure 10(a-d), were used to establish the structure factor used for the kinetic modeling.

As shown in Figure 8(a), the existence of mass transfer limitation during kinetic tests was assessed varying flow rate from 1.5 to 5L/h. Consequently, when the liquid flow rate is less than 3.5 L/h, the EL formation rate increases with the increase of flow rate, confirmed the existence of the external mass transfer limitation. The rate controlling of the esterification reaction is external diffusion, which is the mass transfer process between the liquid phase body and the catalyst surface. The larger the liquid flow rate is, the influence of external mass transfer limitation on the reaction rate is weakened. However, when the flow rate increases to 3.5L/h, the formation rate of EL remains at a certain level. Allowing to conclude that the absence of external mass transfer limitation is evident from larger than 3.5L/h. To eliminate the mass transfer limitation, all the following experiments were performed with a flow rate of 3.5 L/h.

The effect of the AMPD-ZSM-5@SiC was also studied at 3.5L/h and 348.15 K. The structural properties of ZSM-5@SiC used in the experiment are shown in Table S1. Figure 8(b) showed that the EL formation rate of S-ZSM-5@SiC-4 was slightly higher than that of M-ZSM-5@SiC-6. The reason for this phenomenon may be the influence of the average macroscopic pore diameter of S-ZSM-5@SiC-4, the smaller AMPD-ZSM-5@SiC has larger surface areas. Besides, N_2 adsorption-desorption results showed that the specific surface areas of S-ZSM-5@SiC-4 coating and M-ZSM-5@SiC-6 coating were 23.86 and 12.12m^2/g, respectively. NH_3-TPD results presented that the acid active site of structured S-ZSM-5@SiC-4 catalyst is slightly higher than M-ZSM-5@SiC-6. Thus, the higher catalytic performance of S-ZSM-5@SiC-4 can be also attributed to the increase of specific surface areas and acid active site.

The green and blue data in Figure 8(b) represented the catalytic performance of L-ZSM-5@SiC-12 and L-ZSM-5@SiC-13, respectively. To sum up, the effect of the ZSM-5 coating is more significant than the AMPD-ZSM-5@SiC. Therefore, the combined effect of ZSM-5 coating and AMPD-ZSM-5@SiC on the kinetics modeling should be considered.

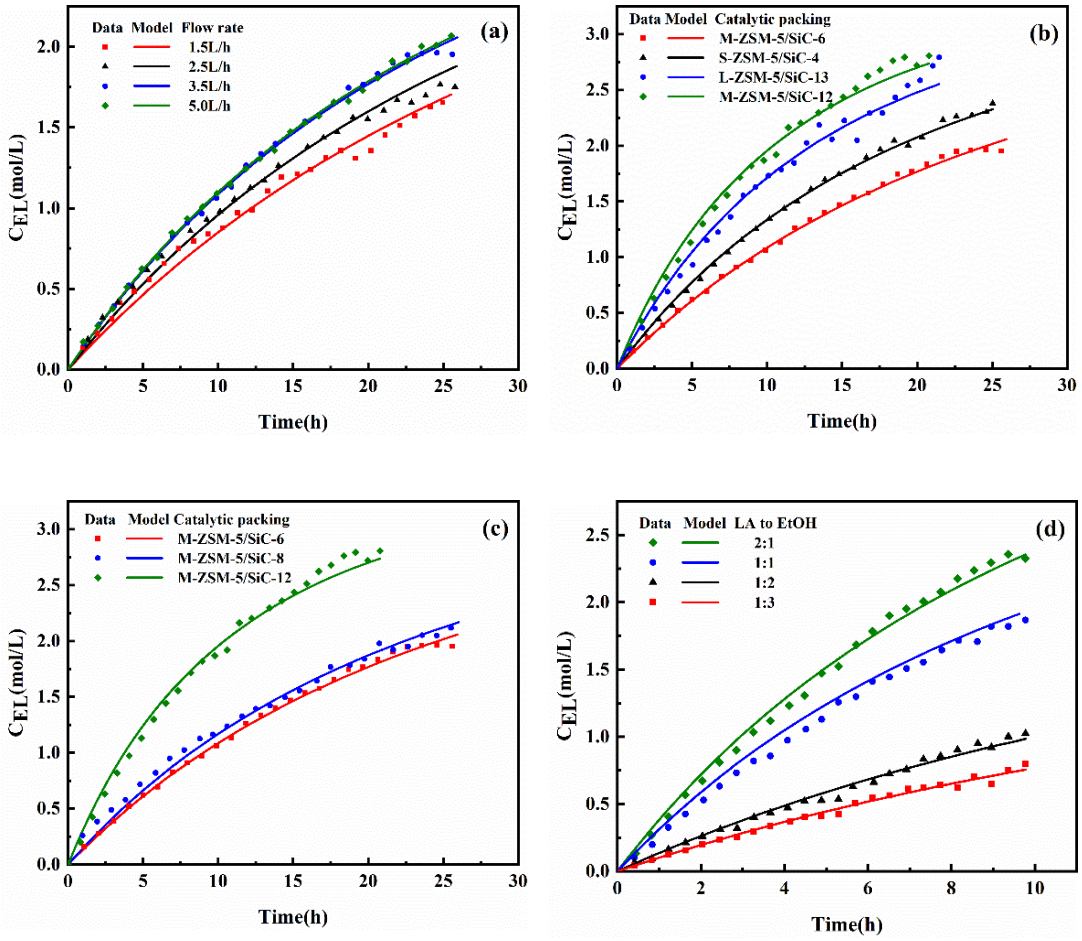

FIGURE 8 (a) Effect of the flow rate on C_{EL}. (Experimental conditions: T=348.15K, Structured catalyst: M-ZSM-5@SiC-6, LA/EtOH=1:1); (b) Effect of the AMPD-ZSM-5@SiC on C_{EL}. (Experimental conditions: T=348.15K, Flow rate =3.5L/h, LA/EtOH=1:1); (c) Effect of ZSM-5 coating thickness on C_{EL}. (Experimental conditions: T=348.15K, Flow rate=3.5L/h, LA/EtOH=1:1); (d) Effect of the molar ratio of LA to EtOH on C_{EL}. (Experimental conditions: T=348.15K, Flow rate =3.5L/h, Structured catalyst: M-ZSM-5@SiC-12); Points are experimental data, while solid lines are model prediction.

Experiments were performed varying the ZSM-5 coating thickness of structured ZSM-5@SiC catalyst keeping other conditions constant. As shown in Figure 8(c), results indicated clearly that a corresponding increase in the reaction rate was observed by increasing the ZSM-5 coating thickness. In addition, we can see a phenomenon that the reaction rate of M-ZSM-5@SiC-12 increases sharply with the increase of the ZSM-5 coating thickness, which is mainly attributed to the sharp increase of the specific surface areas of ZSM-5 coating and acid active site. The specific surface areas of ZSM-5 coating increases from 12.12 to 47.52 m^2/g, and the acid active site increases from 0.04 to 0.22 mmol g^{-1}, which promotes the forward reaction. However, it can be seen that the promotion on the formation rate of EL was less significant with the moderate increase of the coating thickness from the experimental data of M-ZSM-5@SiC-6 and M-ZSM-5@SiC-8. This may be due to the weak acid strength of structured ZSM-5@SiC catalyst. Overall, ZSM-5 coating thickness on the reaction rate has a positive effect, but also brings a series of problems, such as coating uniformity and catalytic performance. Therefore, the appropriate ZSM-5 coating thickness prepared can reduce the heat and mass transfer limitation and improve the catalytic performance.

The dependence of molar ratio of LA to EtOH on the reaction rate was investigated varying from 2:1 to 1:3 keeping all other conditions constant. As presented in Figure 8(d), experimental results show that the EL formation concentration was increased from 0.8 to 2.3 mol/L by varying LA to EtOH mole ratio from 1:3 to 2:1. The reason is that the higher concentration of LA makes the reaction shift in the forward direction. What' more, an interesting phenomenon is that when the molar ratio of LA to EtOH changed from 1:2 to 1:1, the concentration of EL increases sharply. Nevertheless, there are almost negligible EL

concentration improvement varying from 1:1 to 2:1. Compared with the effect of concentration of EtOH, the LA concentration may help improve the reaction rate for the production of EL. This phenomenon may be due to the small acid active site of ZSM-5@SiC acid prepared. However, LA played a role in autocatalysis. In other words, LA could act as not only a reactant but also a catalyst in this esterification process.

To evaluate the structure factor of each experimental condition over structured ZSM-5@SiC catalyst, experimental data were fitting respectively by means of Eqs. (4), (5) and (6). The results from Figure 9 show that the most of the experimental data collected by experiments under different conditions are within the error window of ±20%, confirming again the credibility of the reaction kinetic model established in our study. The structure factors obtained are summarized in Table S7.

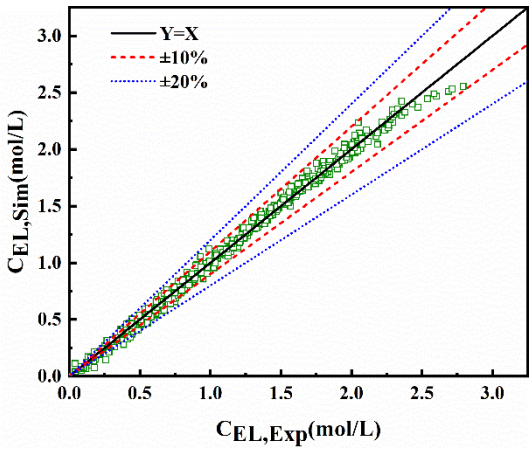

FIGURE 9 Plots of simulated concentration value of EL and the experimental data under operation conditions

4.2.2 | Description of structure factors

The structure factor, a parameter estimated, was introduced into the novel kinetic model to make it more accurately for the design of distillation reactor with ZSM-5@SiC foam

catalytic packing. As can be seen from Table S7, the structure factors are related to many variables. In order to understand the correlation between these variables and structure factors, we have adopted a wholly based on the theory of geometric model to describe this parameter. The functional relationship is shown in Eq. (7):

$$\lambda = f(u, d, \mu_{mix}, \rho_{mix}, d_c, \varepsilon, R_m) \tag{7}$$

where u is the velocity, m/s. d is the AMPD-ZSM-5@SiC, m. μ_{mix} is the mixture viscosity, Pa·s. ρ_{mix} is the mixture density, kg/m^3. d_c is the ZSM-5 coating thickness on the surfaces of SiC-FMS, m. ε is the porosity of structured ZSM-5@SiC catalyst. R_m is the mole ratio of feed LA to EtOH.

The dependence on the liquid density and the viscosity of the temperature can be expressed as Eqs. (8) and (9),[12] which were used to calculate the viscosity's mixing effect.

$$\rho_i = MW_i \frac{A_{\rho i}}{B_{\rho i}^{\left[1+\left(1-\frac{T}{C_{\rho i}}\right)^{D_{\rho i}}\right]}} \tag{8}$$

$$\mu_i = \exp\left[A_{\mu i} + \frac{B_{\mu i}}{T} + C_{\mu i}\ln(T) + D_{\mu i}T\right] \tag{9}$$

where ρ_i and μ_i the density and viscosity of the ith components, respectively. MW_i is the molecular weight of each component, i represent LA, EtOH, EL, and H_2O, respectively. T is the absolute temperature in Kelvin. The other letters are coefficients of the equation, which are reported in Table S8.

As we all known, the pressure loss consists of the viscous and inertial term, which are both functions of the porosity.[35] Furthermore, the pressure loss also affects the kinetics of the reaction similarly. Therefore, Reynolds number is used to express fluid flow situations, and porosity is also correlated in structure factors. Besides, the AMPD-ZSM-5@SiC is related to

its surface areas, and ZSM-5 coating thickness is related to mass transfer limitation, which are integrated with each other in a "Volume-like" form. Finally, the relative influence of Reynolds number and "Volume-like" is comprehensively considered and written in the form of a ratio. The correlation between λ and R_m is referred to work of Gao et al.[20] The assumed structure factor was expressed by the following Eq. (10):

$$\lambda = A + \frac{B(1-\varepsilon)^m \left(\frac{du\rho_{mix}}{\mu_{mix}}\right)^n}{\left[\frac{6d_c(1-\varepsilon)}{d}\right]^q} + C\ln R_m \tag{10}$$

where A, B, C, m, n and q are corresponding constants. The corresponding constants can be determined by multiple linear regression using Levenberg-Marquardt and general global optimization method based on the experimental data. Parameters of the model and the statistical test results for the structure factor were shown in Table 1. The regression coefficient between experimental data and model prediction is found to be 0.983. The very high correlation coefficient value (R^2) indicates an excellent agreement. A parity plot between experimental data and model prediction was presented in Figure 10. This further proves that the assumed structure factor function relation is valid.

TABLE 1 Parameters of the model and the statistical test results for structure factors

Parameter Statistical							Statistical test		
	A	B	C	m	n	q	R^2	RMSE	F
Value	2.894	0.184	0.093	-1.790	-0.312	0.423	0.983	0.11	645

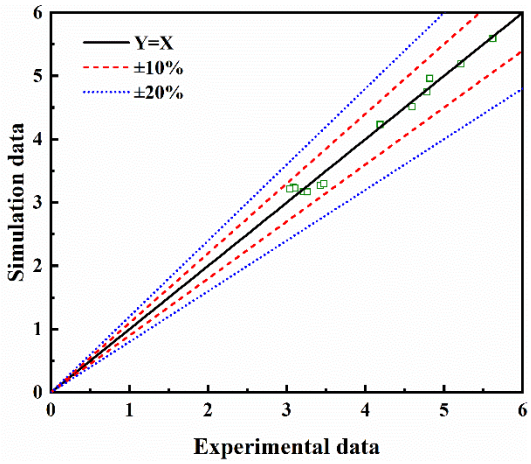

FIGURE 10 Plots of the experimental data and model prediction

The value of these two parameters, namely m and n, are less than zero in parameter's estimation process, which shows that porosity and liquid flow rate have negative effects on the value of λ. It can be found that the smaller λ value is, the more conducive to the forward reaction from the novel kinetic model. The reason why m and n are less than zero might be described as follows: the decrease of porosity represents the increase of surface areas of ZSM-5@SiC, and the reaction rate is related to the contact areas of SiC-FMS. The larger the contact area is, the more beneficial the gas-liquid mass transfer is. This is consistent with the phenomenon that the decrease of λ accelerates the reaction rate. Similarly, the increase of liquid flow rate will lead to the increase of the efficiency of the mass transfer under the same temperature. In addition, the fitting relationship between the inhibition term of reaction kinetics and the coating thickness is also consistent with the experimental trend. Consequently, developed kinetics model with structured ZSM-5@SiC catalyst was listed below:

$$r = 5.006 \times 10^{9} \exp^{\left(\frac{-8776.6}{T}\right)} \frac{\left(a¿¿LA\, a_{EtOH} - a_{EL}\, a_{H_2O} / K_e\right)}{\left(2.894 + \frac{0.184\left(1-\varepsilon\right)^{-1.79}\left(\frac{du\,\rho_{mix}}{\mu_{mix}}\right)^{-0.312}}{\left[\frac{6\,d_c\left(1-\varepsilon\right)}{d}\right]^{0.423}} + 0.093 \ln R_m + 1.245 \times 10^{-9} \exp^{\left(\frac{5787.5}{T}\right)} a_{H_2O}\right.}$$

(11)

5 | DESIGN OF DISTILLATION REACTOR USING DEVELOPED KINETICS

One of the main goals of the kinetic study is to design and optimize distillation reactor (reactive distillation) with catalytic packing based on the structured ZSM-5@SiC catalyst. Since the structure factors of ZSM-5@SiC catalyst are no contained in directive available Aspen Plus, which was incorporated into the process simulator using an additional subroutine written in FORTRAN. What's even more remarkable is that, it is of great significance to consider the difference of liquid flow rate on each theoretical stage into the reaction kinetics model for the matching between of the reaction and separation.

The steady-state simulation of the RD process for design of the distillation reactor has been performed with Aspen Plus embedded FORTRAN. The RadFrac and NRTL model was used in the simulation of the RD process. Binary interaction parameters not included in the Aspen database were estimated using the UNIFAC method. The catalytic packings based on the structured ZSM-5@SiC catalyst were used in the distillation reactor, as shown in Figure 11(a-b), which was consisted of structured corrugated packing and structured ZSM-5@SiC catalyst.

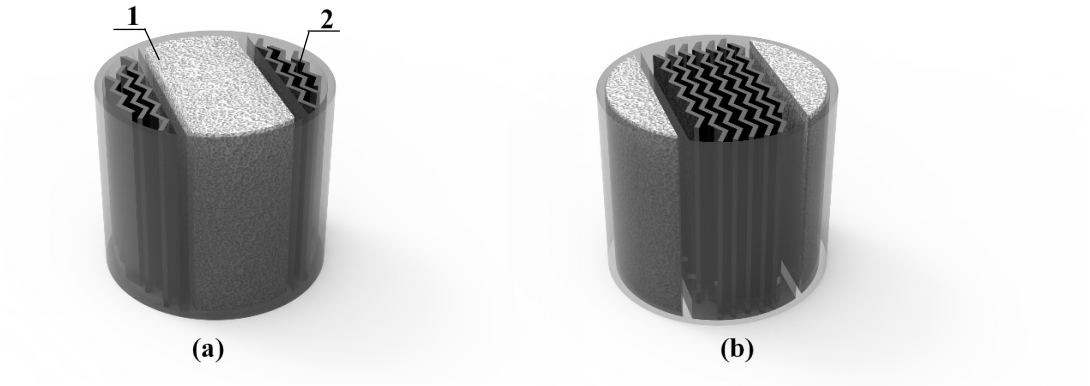

FIGURE 11 (a-b) Graphic model of two structured catalytic packings in the distillation reactor. 1: structured ZSM-5@SiC catalyst, 2: corrugated sheets

The effect of the porosity and the AMPD-ZSM-5@SiC, ZSM-5 coating thickness on the yield of EL and distillation reactor energy consumption per kilogram of EL (Q_{EL})[16] were investigated for evaluating of the EL synthesis efficiency. The input parameters used in the basic case RD process simulation were listed in Table S9.

5.1 | Effect of the porosity of structured ZSM-5@SiC catalyst

The effect of the porosity of structured ZSM-5@SiC catalyst on the yield of EL and distillation reactor energy consumption for the production of EL was investigated for the reactive distillation process of LA. As shown in Figure 12(a), the yield of EL production firstly increases with the decrease in the porosity of structured ZSM-5@SiC catalyst. Then a further decrease in the porosity of structured ZSM-5@SiC catalyst (≤0.5) had no significant contribution to the yield of the EL production, remaining at a certain level (about 37%). Moreover, it can be seen that the energy consumption decreases with the yield of EL production increases. Figure 12(b) shows that the formation rate of EL on each theoretical stage under different porosity of structured ZSM-5@SiC catalyst, which increases gradually from the top to the bottom of the reaction section. According to the kinetics model obtained,

the inhibition terms mainly include structure factor and water concentration, among which the porosity is an important variable affecting the structure factor. The larger the porosity is, the larger the structure factor is, and the more serious the inhibition on the reaction will be, leading to the decrease of the reaction conversion rate. It can be seen from Figure S3 that the change of porosity causes the difference of mass flow of liquid on each stage, which will lead to the difference of corresponding structure factors. Besides, the mass fraction of H_2O on each theoretical stage is shown in Figure S4. We can see that the water concentration is the highest at the top of the reaction section, while the presence of water will inhibit the forward reaction rate. This also verified the higher EL formation rate of the bottom of the reaction section. With the consideration of the yield of EL and distillation reactor energy consumption, the porosity of ZSM-5@SiC catalyst was considered to be 0.55.

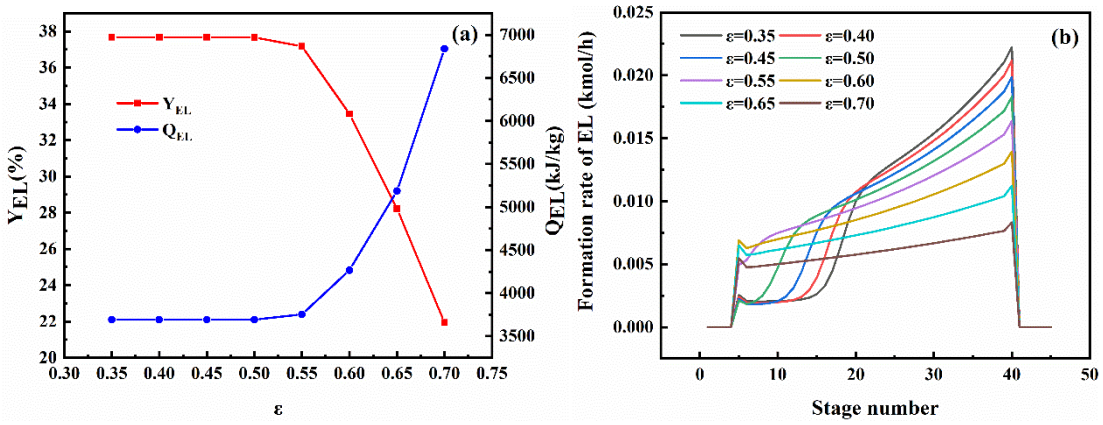

FIGURE 12 (a) Effect of the porosity of structured ZSM-5@SiC catalyst on Y_{EL} and Q_{EL}. (Other conditions: d_c=100μm, d=1mm); (b) Formation rate of EL on each theoretical stage under different porosity of structured ZSM-5@SiC catalyst

5.2 | Effect of the ZSM-5 coating thickness

The effect of the ZSM-5 coating thickness is displayed in Figure 13(a) for the distillation

reactor of LA, which shows the yield of EL increases and distillation reactor energy consumption decreases with an increase in the ZSM-5 coating thickness. It can be primarily attributed to the role of acid active sites in the reaction. Moreover, for the ZSM-5 coating thickness from 150 and 350μm, the yield of EL is approximately the same. The results also confirm the fact that the chemical reaction of catalyst surface is the rate-controlling step, because there is no difference on the yield of EL under the condition of the thicker ZSM-5 coating thickness and higher flow rate. Additionally, an interesting phenomenon can be seen in Figure 13(b), as the thickness of the ZSM-5 coating increases at the top of the reaction section, the formation rate of EL decreases. It can be explained by the mass flow of liquid in Figure 13(c) and the distribution of temperature shown in Figure 13(d) on each theoretical stage. At the top of the reaction section, the lower ZSM-5 coating thickness has a higher temperature and lower flow rate, which indicates that the temperature is the decisive factor in controlling the reaction degree.

However, at the bottom of the reaction section, the difference in mass flow of liquid and distribution of temperature on each theoretical stage can be ignored. The promotion on the yield of EL was significant with the further increase of ZSM-5 coating thickness. In other words, the acid active site (i.e., ZSM-5 coating thickness) is the decisive factor controlling the degree of reaction at this stage. Further, this implies that the mass flow of liquid, temperature distribution, and coating thickness on each theoretical stage have a comprehensive effect on the reaction rate. That is to say, the kinetic model in our research is suitable, showing the mutual restriction relationship between various factors for the design of distillation reactor with ZSM-5@SiC foam catalytic packing. Nevertheless, thicker coating

has a noticeable effect on the internal diffusion, heat and mass transfer, which is unbeneficial to the reaction. Therefore, ZSM-5 coating thickness above 150μm has little influence on the yield of EL, which was took as the choice for simulations.

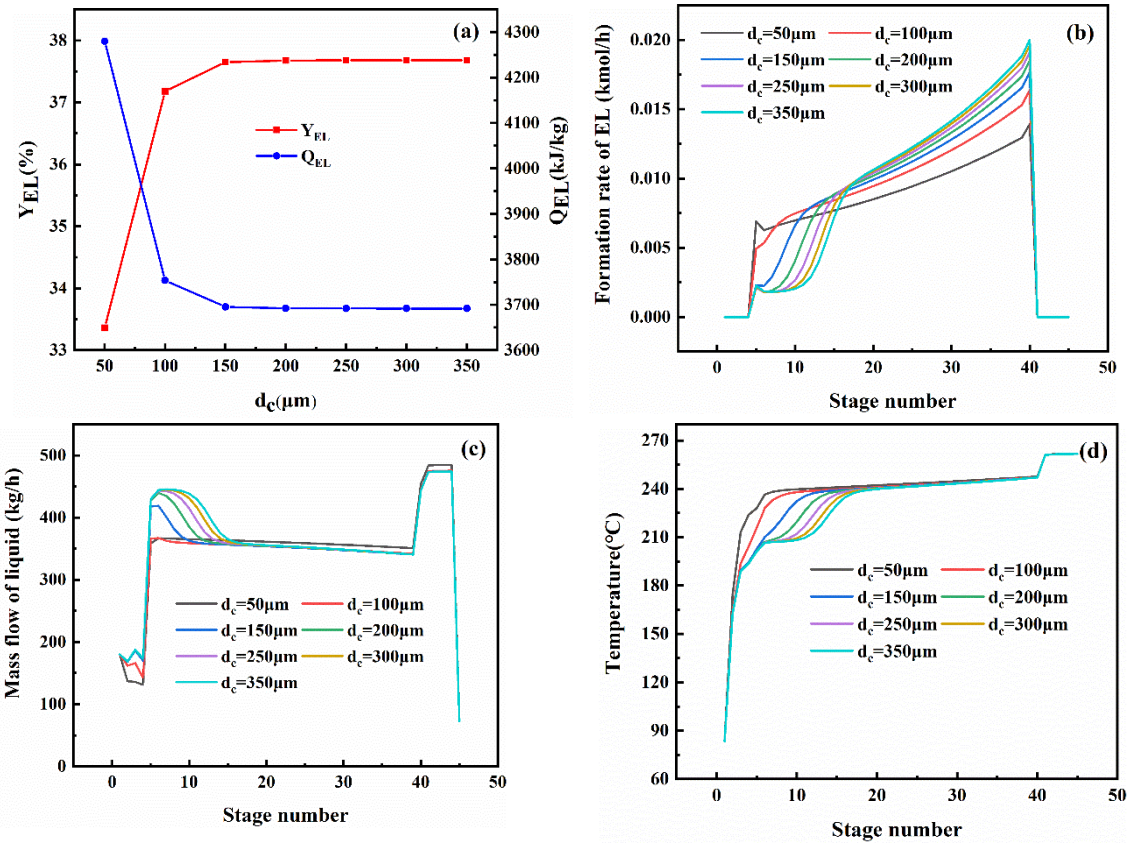

FIGURE 13 (a) Effect of ZSM-5 coating thickness on Y_{EL} and Q_{EL}. (Other conditions: ε=0.55, d=1mm); (b) Formation rate of EL on each theoretical stage under different ZSM-5 coating thickness; (c) Mass flow of liquid on each theoretical stage under different ZSM-5 coating thickness; (d) Distribution of temperature on each theoretical stage under different ZSM-5 coating thickness

5.3 | Effect of the AMPD-ZSM-5@SiC

Figure 14 exhibits that the yield of EL increases trend with a decrease in the AMPD-ZSM-5@SiC. This can be explained by the variation in the surface areas of structured ZSM-5@SiC catalyst, i.e., the smaller the AMPD-ZSM-5@SiC, the higher the surface areas.[35]

Della Torre et al.[46] obtained that the mass transfer coefficient of foam increases with the decrease of pore size by CFD simulation, which indicates that the study of small pore diameter could be helpful for a better reaction rate. Nevertheless, the AMPD-ZSM-5@SiC has a noticeable effect on pressure loss. As the average pore diameter decreases, the pressure drop loss increases. In general, this finding emphasizes that the AMPD-ZSM-5@SiC should be carefully accounted for the accurate design of the structured ZSM-5@SiC foam catalytic packing used for distillation reactor. Here, we selected that the AMPD-ZSM-5@SiC was 1mm due to higher yield of EL and lower pressure drop loss.

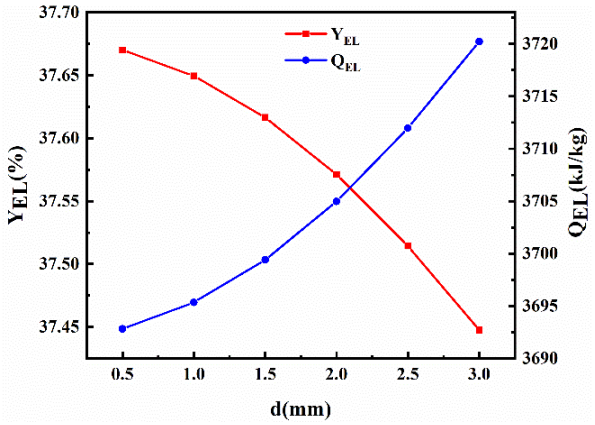

FIGURE 14 Effect of the AMPD-ZSM-5@SiC on Y_{EL} and Q_{EL}. (Other conditions: ε=0.55, d_c=150μm)

In conclusion, the feasibility of the novel kinetic model was verified by RD simulation, which can accurately predict the reaction and separation phenomena to design the distillation reactor with ZSM-5@SiC foam catalytic packing. The optimal the porosity of structured ZSM-5@SiC catalyst in distillation reactor was considered to be 0.55. The thickness of ZSM-5 coating was 150μm and the AMPD-ZSM-5@SiC was 1mm. In this case, the excellent performances of RD in the designed distillation reactor based on the ZSM-5@SiC foam catalytic packing (EL yield 37.65% and distillation reactor energy consumption 3695 kJ/kg)

are achieved.

6 | CONCLUSION

Structured ZSM-5@SiC catalyst with different structures were prepared and used in distillation reactor with catalytic packing for EL synthesis. X-ray CT was used as quantitative analysis of the real pore spatial structure and ZSM-5 coating thickness distribution. The results indicate that the AMPD-ZSM-5@SiC of different samples and the average ZSM-5 coating thickness vary from 0.57 to 1.54mm and 47.7 to 322.45μm, respectively, and further confirm holistic uniform ZSM-5 coating thickness. Microscopic characterizations illustrated that the ZSM-5 coating was successfully grown on the surfaces of SiC-FMS. The catalytic performances were carried out and indicate that the higher EL concentration is obtained at higher temperatures. The larger the liquid flow rate is, the influence of external mass transfer limitation on the reaction rate is weakened. Moreover, the higher concentration of LA makes the reaction shift in the forward direction, and the combined effect of ZSM-5 coating thickness and the AMPD-ZSM-5@SiC should be considered. Furthermore, a novel kinetic model was established by introducing a parameter termed as ‘‘structure factor’’ based on macroscopic properties of structured ZSM-5@SiC catalyst and liquid flow rate in the reactor. The results revealed the model prediction are in good agreement with the experimental data. This further confirms the credibility of the reaction kinetic model established in this work. In addition, distillation reactor simulations have been performed based on the developed kinetics model, which was incorporated into Aspen Plus embedded FORTRAN. The optimal the porosity of structured ZSM-5@SiC catalyst in distillation reactor was considered to be 0.55. The thickness of ZSM-5 coating was 150μm and the AMPD-ZSM-5@SiC was 1mm. In this

case, the excellent performances of RD in the designed distillation reactor based on the ZSM-5@SiC foam catalytic packing (EL yield 37.65% and distillation reactor energy consumption 3695 kJ/kg) are achieved.

To some extent, such findings in this work could serve as a tool for further design of the distillation reactor with ZSM-5@SiC foam catalytic packing. Nevertheless, the catalytic performance of the prepared ZSM-5@SiC catalyst still needs to be improved. In the future, we will work on further optimization of the acid active site of the ZSM-5@SiC and kinetic model (e.g., the microstructure of catalyst) for achieving a higher-yield and economical distillation reactor with ZSM-5@SiC foam catalytic packing for EL synthesis in industrial scale.

ACKNOWLEDGMENTS

The authors acknowledge financial support from National Key R&D Program of China (2019YFE0123200) and National Nature Science Foundation of China (Nos. 21776202, 22078348, 61771328). The authors also thank the reviewers for their insightful comments and suggestions.

REFERENCES

1. Kong X, Wu S, Liu L, Li S, Liu J. Continuous synthesis of ethyl levulinate over Cerium exchanged phosphotungstic acid anchored on commercially silica gel pellets catalyst. *Mol Catal.* 2017;439:180-185.
2. Patil CR, Niphadkar PS, Bokade VV, Joshi PN. Esterification of levulinic acid to ethyl levulinate over bimodal micro–mesoporous H/BEA zeolite derivatives. *Catal Commun*. 2014;43:188-191.
3. Pavlovic J, Popova M, Mihalyi RM, Mazaj M, Mali G, Kovač J, Lazarova H, Rajic N.

Catalytic activity of SnO2- and SO4/SnO2-containing clinoptilolite in the esterification of levulinic acid. *Micropor Mesopor Mater.* 2019;279:10-18.

4. Russo V, Hrobar V, Mäki-Arvela P, Eränen K, Sandelin F, Di Serio M, Salmi T. Kinetics and Modelling of Levulinic Acid Esterification in Batch and Continuous Reactors. *Top Catal.* 2018;61(18-19):1856-1865.
5. Windom BC, Lovestead TM, Mascal M, Nikitin EB, Bruno TJ. Advanced Distillation Curve Analysis on Ethyl Levulinate as a Diesel Fuel Oxygenate and a Hybrid Biodiesel Fuel. *Energy Fuels*. 2011;25(4):1878-1890.
6. Quereshi S, Ahmad E, Pant KK, Dutta S. Insights into the metal salt catalyzed ethyl levulinate synthesis from biorenewable feedstocks. *Catal Today*. 2017;291:187-194.
7. Liu H, Zhang Y, Hou T, Chen X, Gao C, Han L, Xiao W. Mechanical deconstruction of corn stover as an entry process to facilitate the microwave-assisted production of ethyl levulinate. *Fuel Process Technol.* 2018;174:53-60.
8. Xu G, Chang C, Fang S, Ma X. Cellulose reactivity in ethanol at elevate temperature and the kinetics of one-pot preparation of ethyl levulinate from cellulose. *Renew Energ.* 2015;78:583-589.
9. Cirujano FG, Corma A, Llabrés i Xamena FX. Conversion of levulinic acid into chemicals: Synthesis of biomass derived levulinate esters over Zr-containing MOFs. *Chem Eng Sci.* 2015;124:52-60.
10. Fernandes DR, Rocha AS, Mai EF, Mota CJA, Teixeira da Silva V. Levulinic acid esterification with ethanol to ethyl levulinate production over solid acid catalysts. *Appl Catal A: Gen.* 2012;425-426:199-204.
11. Kuwahara Y, Fujitani T, Yamashita H. Esterification of levulinic acid with ethanol over sulfated mesoporous zirconosilicates: Influences of the preparation conditions on the structural properties and catalytic performances. *Catal Today*. 2014;237:18-28.

12. Russo V, Rossano C, Salucci E, Tesser R, Salmi T, Di Serio M. Intraparticle diffusion model to determine the intrinsic kinetics of ethyl levulinate synthesis promoted by Amberlyst-15. *Chem Eng Sci.* 2020;228:115974.
13. Russo V, Tesser R, Rossano C, Cogliano T, Vitiello R, Leveneur S, Di Serio M. Kinetic study of Amberlite IR120 catalyzed acid esterification of levulinic acid with ethanol: From batch to continuous operation. *Chem Eng J.* 2020;401:126126.
14. Neves P, Lima S, Pillinger M, Rocha SM, Rocha J, Valente AA. Conversion of furfuryl alcohol to ethyl levulinate using porous aluminosilicate acid catalysts. *Catal Today*. 2013;218-219:76-84.
15. Li X, Lai J, Cong H, Shu C, Zhao R, Wang Y, Li H, Gao X. Toward sustainable and eco-efficient novel catalytic distillation process for production of solketal using seepage catalytic packing internal. *Catal Today*. 2020.
16. Li X, Zhang Q, Li H, Gao X. A Novel Process for the Production of Triethylene Glycol Di-2-ethylhexoate by Reactive Distillation Using a Sulfated Zirconia Catalyst. *Ind Eng Chem Res.* 2020;59(19):9242-9253.
17. Kiss AA, Jobson M, Gao X. Reactive Distillation: Stepping Up to the Next Level of Process Intensification. *Ind Eng Chem Res.* 2018;58(15):5909-5918.
18. Gao X, Zhao R, Cong H, Na J, Shi Y, Li H, Li X. Reactive Distillation toward an Ecoefficient Process of Continuous Biodiesel Manufacture from Waste Oil: Pilot-Scale Experiments and Process Design. *Ind Eng Chem Res*. 2020;59(33):14935-14946.
19. Li H, Xiao C, Li X, Gao X. Synthesis of n-Amyl Acetate in a Pilot Plant Catalytic Distillation Column with Seepage Catalytic Packing Internal. *Ind Eng Chem Res*. 2017;56(44):12726-12737.
20. Gao X, Li X, Li H. Hydrolysis of methyl acetate via catalytic distillation: Simulation and design of new technological process. *Chem Eng Process*. 2010;49(12):1267-1276.

21. Li X, Wu Y, Li H, Yuan G, Chen H, Gao X. Intensification of 2-Methyl-1,3-Dioxolane hydrolysis for recovery of ethylene glycol through reactive distillation: Kinetics and process design. *Chem Eng Process*. 2020;154:108012.

22. Onkarappa SB, Javoor M, Mal SS, Dutta S. Efficient and Scalable Production of Alkyl Levulinates from Cellulose-Derived Levulinic Acid Using Heteropolyacid Catalysts. *ChemistrySelect*. 2019;4(8):2501-2504.

23. Caetano MG, González JC, Solari RB. Flowdynamic Modeling of Bale−Type Catalytic Distillation Packings. *Separ Sci Technol*. 2005;39(4):855-877.

24. Manduca E, González JC, Elman H. Mass Transfer Characteristics of Bale-Type Catalytic Distillation Packings. *Separ Sci Technol*. 2003;38(14):3535-3552.

25. Ratheesh S, Kannan A. Holdup and pressure drop studies in structured packings with catalysts. *Chem Eng J.* 2004;104(1-3):45-54.

26. Gorak A, Hoffmann A, Catalytic distillation in structured packings Methyl acetate synthesis. *AICHE J.* 2001;47(5): 1067-1076

27. Deng T, Ding J, Zhao G, Liu Y, Lu Y. Catalytic distillation for esterification of acetic acid with ethanol: promising SS−fiber@HZSM−5 catalytic packings and experimental optimization via response surface methodology. *J Chem Technol Biotechnol*. 2017;93(3):827-841.

28. Deng T, Zhao G, Liu Y, Lu Y. Catalytic distillation for one-step cyclohexyl acetate production and cyclohexene-cyclohexane separation via esterification of cyclohexene with acetic acid over microfibrous-structured Nafion-SiO2/SS-fiber packings. *Chem Eng Process*. 2018;131:215-226.

29. Chen H, Shao Y, Mu Y, Xiang H, Zhang R, Chang Y, Hardacre C, Wattanakit C, Jiao Y, Fan X. Structured silicalite−1 encapsulated Ni catalyst supported on SiC foam for dry reforming of methane. *AIChE J*. 2020; e17126.

30. Jiao Y, Fan X, Perdjon M, Yang Z, Zhang J. Vapor-phase transport (VPT) modification of ZSM-5/SiC foam catalyst using TPAOH vapor to improve the methanol-to-propylene (MTP) reaction. *Appl Catal A: Gen.* 2017;545:104-112.

31. Jiao Y, Jiang C, Yang Z, Liu J, Zhang J. Synthesis of highly accessible ZSM-5 coatings on SiC foam support for MTP reaction. *Micropor Mesopor Mater.* 2013;181:201-207.

32. Jiao Y, Jiang C, Yang Z, Zhang J. Controllable synthesis of ZSM-5 coatings on SiC foam support for MTP application. *Micropor Mesopor Mater.* 2012;162:152-158.

33. Jiao Y, Yang X, Jiang C, Tian C, Yang Z, Zhang J. Hierarchical ZSM-5/SiC nano-whisker/ SiC foam composites: Preparation and application in MTP reactions. *J Catal*. 2015;332:70-76.

34. Zhang R, Chen H, Mu Y, Chansai S, Ou X, Hardacre C, Jiao Y, Fan X. Structured Ni@ NaA zeolite supported on silicon carbide foam catalysts for catalytic carbon dioxide methanation. *AIChE J*. 2020;66: e17007.

35. Bracconi M, Ambrosetti M, Okafor O, Sans V, Zhang X, Ou XX, Da Fonte CP, Fan XL, Maestri M, Groppi G, Tronconi E. Investigation of pressure drop in 3D replicated open-cell foams：Coupling CFD with experimental data on additively manufactured foams. *Chem Eng J*. 2018;377:120123.

36. Li H, Fu L, Li X, Gao X. Mechanism and analytical models for the gas distribution on the SiC foam monolithic tray. *AIChE J.* 2015;61(12):4509-4516.

37. Chen H, Yan Y, Shao Y, Zhang H, Chen H. Catalytic combustion kinetics of isopropanol over novel porous microfibrous-structured ZSM-5 coating/PSSF catalyst. *AIChE J.* 2015;61(2): 620-630.

38. Wen M, Ding J, Wang C, Li Y, Zhao G, Liu Y, Lu Y. High-performance SS-fiber@HZSM-5 core–shell catalyst for methanol-to-propylene: A kinetic and modeling

study. *Micropor Mesopor Mater.* 2016;221:187-196.

39. Kong L, Ostadhassan M, Li C, Tamimi N. Pore characterization of 3D-printed gypsum rocks: a comprehensive approach. *J Mater Sci*. 2018;53(7):5063-5078.
40. Gao X, Ding Q, Wu Y, Jiao Y, Zhang J, Li X, Li H. Kinetic study of esterification over structured ZSM-5-coated catalysts based on fluid flow situations in macrocellular foam materials. *Reac Chem Eng*. 2020;5(3):485-494.
41. Steinigeweg S, Gmehling J. Esterification of a Fatty Acid by Reactive Distillation. *Ind Eng Chem Res*. 2003;42:3612-3619.
42. Chandra Shekara BM, Ravindra Reddy C, Madhuranthakam CR, Jai Prakash BS, Bhat YS. Kinetics of Esterification of Phenylacetic Acid withp-Cresol over H-β Zeolite Catalyst under Microwave Irradiation. *Ind Eng Chem Res.* 2011;50(7):3829-3835.
43. Schildhauer TJ, Hoek I, Kapteijn F, Moulijn JA. Zeolite BEA catalysed esterification of hexanoic acid with 1-octanol: Kinetics, side reactions and the role of water. *Appl Catal A: Gen.* 2009;358(2):141-145.
44. Li H, Wu C, Zhang Q, Li X, Gao X. Synthesis of 1,3-Dioxolane from Aqueous Formaldehyde Solution and Ethylene Glycol: Kinetics and Reactive Distillation. *Ind Eng Chem Res*. 2019;58(17):7025-7036.
45. Yang P, Li X, Li H, Cong H, Kiss A, Gao, X. Unraveling the influence of residence time distribution on the performance of reactive distillation – process optimization and experimental validation. *Chem Eng Sci*. 2021.(Accepted).
46. Della Torre A, Lucci F, Montenegro G, Onorati A, Dimopoulos Eggenschwiler P, Tronconi E, Groppi G. CFD modeling of catalytic reactions in open-cell foam substrates. *Comput Chem Eng*. 2016;92:55-63.